Nano Energy (2014) 8, 150–156

Available online at www.sciencedirect.com

ScienceDirect

journal homepage: www.elsevier.com/locate/nanoenergy

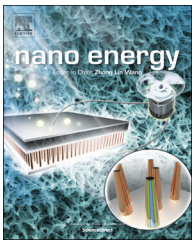

RAPID COMMUNICATION

Simulation method for optimizing the performance of an integrated triboelectric nanogenerator energy harvesting system

Simiao Niu[a], Yu Sheng Zhou[a], Sihong Wang[a], Ying Liu[a], Long Lin[a], Yoshio Bando[b], Zhong Lin Wang[a,b,*]

[a]School of Materials Science and Engineering, Georgia Institute of Technology, Atlanta, GA 30332-0245, United States
[b]Satellite Research Facility, MANA, International Center for Materials Nanoarchitectonics, National Institute for Materials Science, 1-1 Namiki, Tsukuba 305-0044, Japan

Received 13 May 2014; accepted 29 May 2014
Available online 6 June 2014

KEYWORDS
Mechanical energy harvesting;
Triboelectric nanogenerators;
Equivalent circuits;
Simulation method;
Integrated systems

Abstract
Demonstrating integrated triboelectric nanogenerator energy harvesting systems that contain triboelectric nanogenerators, power management circuits, signal processing circuits, energy storage elements, and/or load circuits are core steps for practical applications of triboelectric nanogenerators. Through the design flow of such systems, theoretical simulation plays a critical role. In this manuscript, we provided a new theoretical simulation method for integrated triboelectric nanogenerator systems through integrating the equivalent circuit model of triboelectric nanogenerators into SPICE software. This new simulation method was validated by comparing its results with analytical solutions in some specific triboelectric nanogenerator systems. Finally, we employed this new simulator to analyze the performance of an integrated triboelectric nanogenerator system with a power management circuit. From the study of the influence of different circuit parameters, we outline the design strategy for such kind of triboelectric nanogenerator systems.

Introduction

Scavenging ambient mechanical energy from the environment has long been considered as a critical research topic [1–5]. Recently, triboelectric nanogenerators (TENGs) based

*Corresponding author at: School of Materials Science and Engineering, Georgia Institute of Technology, Atlanta, GA 30332-0245, United States.
E-mail address: zlwang@gatech.edu (Z.L. Wang).

http://dx.doi.org/10.1016/j.nanoen.2014.05.018
2211-2855/

on contact electrification [6-8] and electrostatic induction emerge as a promising technology of mechanical energy harvesting, especially for powering portable electronics [9-14] or working as self-powered sensors [15]. Similar to the development of CMOS integrated circuits and systems, the fully-integrated energy harvesting systems that contain TENGs, power management circuits, signal processing circuits, energy storage elements, and/or load circuits are essential for the practical applications of the TENGs. Theoretical simulation plays a key role in understanding the working mechanism and analyzing the output performance of the TENGs, which paves the way for future design and optimization of the entire system. In this regard, a few efforts have been made to carry out the numerical calculations and analytical studies on the output characteristics of the TENG unit with various working modes [16-19]. However, all the prior investigations merely focus on the behavior of TENG itself, or simply with linear resistive load circuits, while the even more complex analysis with practical load circuits that contain arbitrary numbers of linear and non-linear components could hardly be accomplished by the currently-established simulation approaches. Therefore, a new simulation method of TENGs is highly desired to solve the challenges in the calculations of practical energy harvesting systems.

In this manuscript, the first equivalent circuit model of TENGs was derived to deepen the understanding of their core physics and assist their simulation process. Then the first simulator of an entire TENG system was built by integrating the TENG equivalent circuit model into circuit design software (commonly called SPICE software). The effectiveness of this simulator was validated by comparing its results with analytical solutions in some specific triboelectric nanogenerator systems. Then to show the potential application of this powerful new method, we studied the performance of a TENG with a power management system and outlined the strategy for the design of such system for optimum performance. The new TENG simulator demonstrated in this paper is not only a standard tool for theoretically analyzing the output characteristics of TENGs in any complex systems, but also provides a novel approach for optimum design of the TENG-based energy harvesting systems. This research will lead to fast development of the TENG's performance, and accelerate the process for its practical applications and commercialization.

Results and discussion

As a common sense, the equivalent circuit model is one of the most important theoretical understandings of an electronic device. Similar to the Ebers-Moll model (EM model) [20] of bipolar transistors that is derived from their governing equation, the equivalent circuit model of TENGs can also be derived from their governing equation (V-Q-x relationship), as shown below [16,17]

$$V = -\frac{1}{C_{TENG}}Q + V_{OC} \tag{1}$$

From Eq. (1), there are two terms at the right side, which can be represented by two circuit elements in the equivalent circuit model. The first one is a capacitance term, which is originated from the capacitance between the two electrodes and can be represented by a capacitor (C_{TENG}). The other is an open-circuit voltage term, which is originated from the separation of the polarized tribo-charges and can be represented by an ideal voltage source (V_{OC}). In combination of these two, the whole equivalent circuit model can be represented by a serial connection of an ideal voltage source and a capacitor, as shown in Figure 1.

The above equivalent circuit model is very helpful to understand the core physics of TENGs. For example, the optimum resistance [16] and three-working-region behavior [16] can be easily understood from this equivalent circuit model, which is inherently because of the impedance match between C_{TENG} and the load resistance. The inherent capacitance of TENG will show impedance to the AC voltage source V_{OC}. Any structural parameters that will increase this inherent capacitance will lower this impedance and thus lower the matched resistance. Increasing the velocity of motion is equivalent of increasing the frequency of the AC voltage source V_{OC} so the matched resistance will also be lowered. Since the impedance of C_{TENG} is independent of the tribo-charge density, the matched load resistance is also not affected by the tribo-charge density.

This equivalent circuit model extraction is also the first step of building this new TENG simulator. After the equivalent circuit model is obtained, the values of the ideal voltage source and the capacitance in the above equivalent circuit model need to be specified to complete this integration to the SPICE software. From the basic electrodynamics theory, both V_{OC} and C_{TENG} are only functions of the moving distance (x) and structural parameters while independent of motion parameters, such as velocity and acceleration [16-19]. Two methods are currently developed to specify the V_{OC}-x and C_{TENG}-x relationships. Analytical derivation is a preferred method but it only works for certain geometry features such as parallel plate contact-mode or sliding-mode TENGs. A more general method which works for all TENGs is numerical calculation based on finite element method (FEM). In this method, the value of V_{OC} and C_{TENG} is first obtained at certain values of x. Then, from continuous fraction interpolation, a numerical V_{OC}-x and C_{TENG}-x relationship can be generated in the entire x region.

Now the TENG can be embedded into the SPICE software as a basic element consisting of a voltage source in serial connection with a capacitor. To simulate the whole system in SPICE, several other steps are needed, including inserting other circuit elements, specifying the $x(t)$ relationship that represents the mechanical motion input, as well as initializing

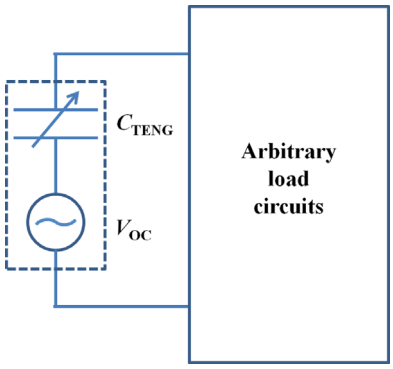

Figure 1 Equivalent circuit model of a triboelectric nanogenerator.

the storage elements. For example, residue charges of triboelectric nanogenerators at initial condition ($t=0$) can be represented by the initial voltage across the capacitor C_{TENG}.

After the system is set in SPICE, the transit analysis of the TENG system can be performed. To validate the results from the SPICE software, we started with some TENG systems that can be solved analytically and the comparison of the results obtained from both methods is shown in Figure 2.

The first example is a parallel plate sliding-mode triboelectric nanogenerator loaded with a resistor. The parameters utilized in this calculation are listed in Table 1. The top plate of this triboelectric nanogenerator is under a constant velocity condition with the maximum moving distance within the range of the bottom plate and the motion process is shown below.

$$x = vt\left(t \le \frac{x_{max}}{v}\right) \tag{2}$$

From our previous analysis, the governing equation of this whole system combining the TENG and the resistor can be given as [17]:

$$R\frac{dQ}{dt} = V = -\frac{1}{C_{TENG}}Q + V_{OC} = -\frac{d_0}{w\varepsilon_0(l-x)}Q + \frac{\sigma d_0 x}{\varepsilon_0(l-x)} \tag{3}$$

With the boundary condition of $Q\ (t=0)=Q_0$ (the initial charges on the plates of triboelectric nanogenerators are Q_0), the output voltage and current of the resistor can be obtained analytically by solving the above differential equation, as shown below [17]:

$$I = \sigma w v \frac{d_0}{Rw\varepsilon_0 v - d_0}\left\{\frac{l}{l-vt}\exp\left[\frac{d_0}{Rw\varepsilon_0 v}\ln\left(\frac{l-vt}{l}\right)\right] - 1\right\} - Q_0\exp\left[\frac{d_0}{Rw\varepsilon_0 v}\ln\left(\frac{l-vt}{l}\right)\right]\frac{d_0}{Rw\varepsilon_0(l-vt)} \quad \left(t \le \frac{x_{max}}{v}\right) \tag{4}$$

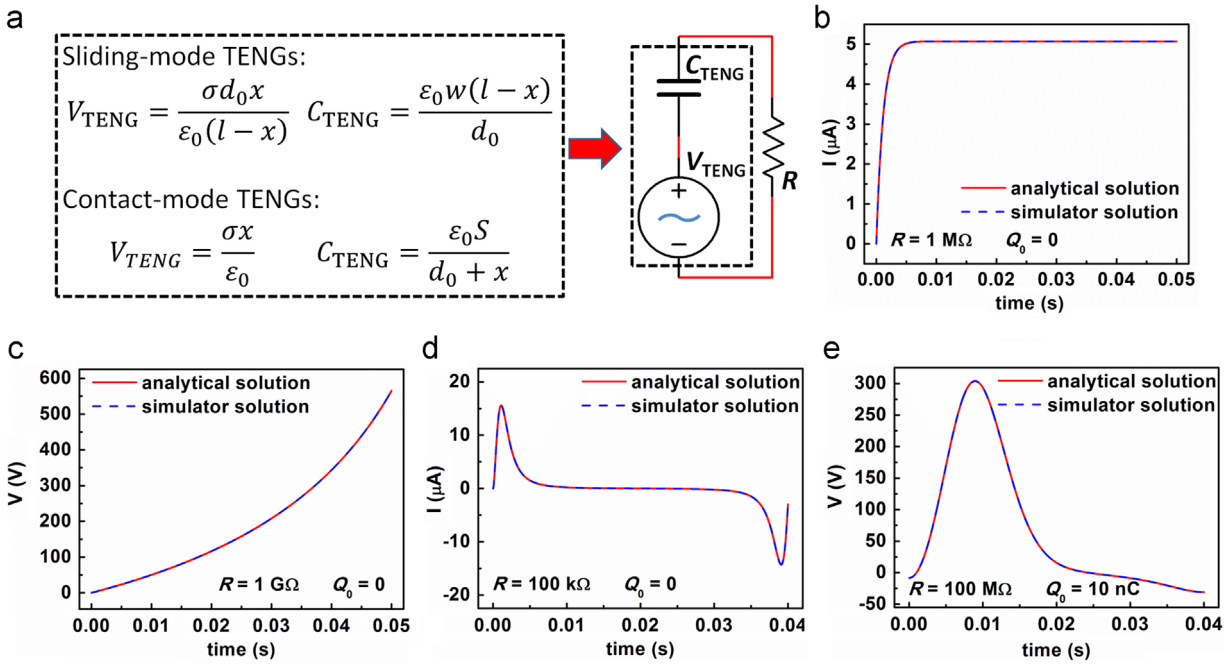

Figure 2 Verification of the built simulator. (a) Equations of contact and sliding-mode TENGs and equivalent circuits for the whole TENG system loaded by a resistor (b-e) Comparisons of outputs from the simulator and analytical equation. (b) Current output comparison under 1 MΩ load and $Q_0=0$ conditions for the sliding-mode TENG. (c) Voltage output comparison under 1 GΩ load and $Q_0=0$ conditions for the sliding-mode TENG. (d) Current output comparison under 100 kΩ load and $Q_0=0$ conditions for the contact-mode TENG. (e) Voltage output comparison under 100 MΩ load and $Q_0=10$ nC conditions for the contact-mode TENG.

Table 1 Parameters of the TENGs utilized to validate the new simulator.

	Sliding-mode TENG	Contact-mode TENG
Dielectric 1	$\varepsilon_{r1}=4$, $d_1=125$ μm	$\varepsilon_{r1}=3.4$, $d_1=125$ μm
Dielectric 2	Metal, $d_2=0$ μm	Metal, $d_2=0$ μm
Effective dielectric thickness	$d_0=d_1/\varepsilon_{r1}+d_2/\varepsilon_{r2}=31.25$ μm	$d_0=d_1/\varepsilon_{r1}+d_2/\varepsilon_{r2}=36.76$ μm
Width of dielectrics w	0.05 m	0.05 m
Length of dielectrics l	0.08 m	0.1 m
Tribo-charge surface density σ	100 μCm^{-2}	8 μCm^{-2}
Maximum separation distance x_{max}	0.05 m	0.002 m
Velocity v	1 ms^{-1}	0.1 ms^{-1}

$$V = \sigma w v R \frac{d_0}{Rw\varepsilon_0 v - d_0}\left\{\frac{l}{l-vt}\exp\left[\frac{d_0}{Rw\varepsilon_0 v}\ln\left(\frac{l-vt}{l}\right)\right]-1\right\} - Q_0\exp\left[\frac{d_0}{Rw\varepsilon_0 v}\ln\left(\frac{l-vt}{l}\right)\right]\frac{d_0}{w\varepsilon_0(l-vt)} \quad \left(t \le \frac{x_{max}}{v}\right) \tag{5}$$

Real-time outputs from the simulator for some specific values for R and Q_0 are plotted in Figure 2b and c, with comparison of the analytical results obtained from Eqs. (4) and (5). From these figures, we can observe that both methods show exactly the same solution for any load resistances and initial condition.

The second and a more complicated example is a parallel plate contact-mode triboelectric nanogenerator loaded with a resistor. The parameters used in this calculation are listed in Table 1. To be more accurate to the real experimental conditions, the top plate of this triboelectric nanogenerator is set to move in a simple harmonic mode as described below.

$$x = \frac{x_{max}}{2} - \frac{x_{max}}{2}\cos\left(\frac{\pi v}{x_{max}}t\right) \tag{6}$$

From our previous analysis, the governing equation of this whole system combining the triboelectric nanogenerators and the resistor can be given as [16]:

$$R\frac{dQ}{dt} = V = -\frac{1}{C_{TENG}}Q + V_{OC} = -\frac{d_0 + x}{\varepsilon_0 wl}Q + \frac{\sigma x}{\varepsilon_0} \tag{7}$$

With the boundary condition of $Q\,(t=0)=Q_0$, the analytical results of output voltage and current can be given as [16]:

$$I(t) = -\frac{\sigma d_0}{R\varepsilon_0} + \frac{2d_0 + x_{max} - x_{max}\cos((\pi v/x_{max})t)}{2Rwl\varepsilon_0} \times\exp\left[-\frac{1}{Rwl\varepsilon_0}\left(d_0 t + \frac{x_{max}}{2}t - \frac{{x_{max}}^2}{2\pi v}\sin\left(\frac{\pi v}{x_{max}}t\right)\right)\right] \times\left\{\sigma wl - Q_0 + \frac{\sigma d_0}{R\varepsilon_0}\int_0^t \exp\left[\frac{1}{Rwl\varepsilon_0}\left(d_0 z + \frac{x_{max}}{2}z - \frac{{x_{max}}^2}{2\pi v}\sin\left(\frac{\pi v}{x_{max}}z\right)\right)\right]dz\right\} \tag{8}$$

$$V(t) = -\frac{\sigma d_0}{\varepsilon_0} + \frac{2d_0 + x_{max} - x_{max}\cos((\pi v/x_{max})t)}{2wl\varepsilon_0} \times\exp\left[-\frac{1}{Rwl\varepsilon_0}\left(d_0 t + \frac{x_{max}}{2}t - \frac{{x_{max}}^2}{2\pi v}\sin\left(\frac{\pi v}{x_{max}}t\right)\right)\right] \times\left\{\sigma wl - Q_0 + \frac{\sigma d_0}{R\varepsilon_0}\int_0^t \exp\left[\frac{1}{Rwl\varepsilon_0}\left(d_0 z + \frac{x_{max}}{2}z - \frac{{x_{max}}^2}{2\pi v}\sin\left(\frac{\pi v}{x_{max}}z\right)\right)\right]dz\right\} \tag{9}$$

These equations are very complex, from which obtaining numerical outputs can only be achieved through complicated numerical calculation methods. As a comparison, a numerical output solution can be easily obtained from the simulator we built above, which is plotted in Figure 2d and e together with the analytical results from Eqs. (8) and (9). Similar to the above comparison, the simulator provides almost the same results with the analytical solution.

Above we provided two simple examples to show the validity of this newly-built simulator. In these cases, this integrated simulator can provide the correct results with a much easier-to-use interface. However, the application of this simulator is much more beyond these two simple examples. In real applications, first, the load circuits are usually a combination of linear and nonlinear elements, including resistors, diodes (rectifiers), transistors, capacitors, inductors (transformers), and so forth. Besides, the real mechanical motion could be quite irregular. Moreover, the triboelectric nanogenerator itself is not so ideal and cannot be analytically represented. In such circumstances, utilizing the analytical method to solve non-linear differential equation sets is nearly an impossible task (See supporting information for a practically unsolvable example of the analytical method). Therefore, utilizing this new simulator is the only way to handle these practical problems and below we will provide an example that utilizing this simulator to design an on-chip power management system for triboelectric nanogenerators.

Because of the inherent capacitive characteristics [17], TENGs can only provide unstable AC voltage/current outputs, which is undesirable for most portable electronic applications. Therefore, a power management circuit is very necessary to convert these AC outputs from TENGs to DC outputs. Figure 3b shows a typical TENG power management circuit [21], including a diode bridge rectifier (D_1 to D_4, parameters shown in Table S1) and a filter capacitor (C_L). The resistive load is now represented by a load resistor R_L, which is in parallel connected with the filter capacitor. As an example, the TENG in this system is a parallel-plate contact-mode TENG with the parameter given in Table 1. Same as above, the top plate of this TENG is also under the same cosine motion. With the initial condition of $Q\,(t=0)=Q_0=0$ and no charges on the filter capacitor, the output of the whole circuit can be simulated by the simulator.

The output voltage curves under $C_L=10$ μF and $R_L=10$ kΩ, 100 kΩ are shown in Figure 3c and d, respectively. Since there are no initial charges on the filter capacitor C_L, both of these two circumstances has a transition state, during which the capacitor is under charging. After several seconds, the transition state ends while the output goes to a periodic steady state, which has the same period as the mechanical motion. This periodic voltage signal is the steady state output signal, which has a DC component (V_{DC}) and a ripple component (v_{ripple}). The DC component of the output is dependent on the load resistance. For example, under $R_L=100$ kΩ condition, the DC component of the output is 0.185 V, much larger than 0.0187 V, the DC component when $R_L=10$ kΩ. Besides the DC component, there is also an undesirable ripple component in the output, which affects the stability of the output as a DC power source. The stability of the output under $R_L=100$ kΩ condition is much better than that under $R_L=10$ kΩ condition. Quantitatively, this stability is shown by the ripple factor (f_r), defined as the ratio between the effective value of v_{ripple} and V_{DC}. f_r under $R_L=100$ kΩ condition is 0.86%, which is much smaller than that under $R_L=10$ kΩ condition (8.61%).

To systematically understand the influence of the filter capacitance and the load resistance on the output performance, the output under several filter capacitances and load resistances is calculated and the corresponding DC voltage, average power, and ripple factor are plotted in Figure 4a-c. As shown in Figure 4a, V_{DC} quickly increases with the increase of R_L when R_L is small. However, due to

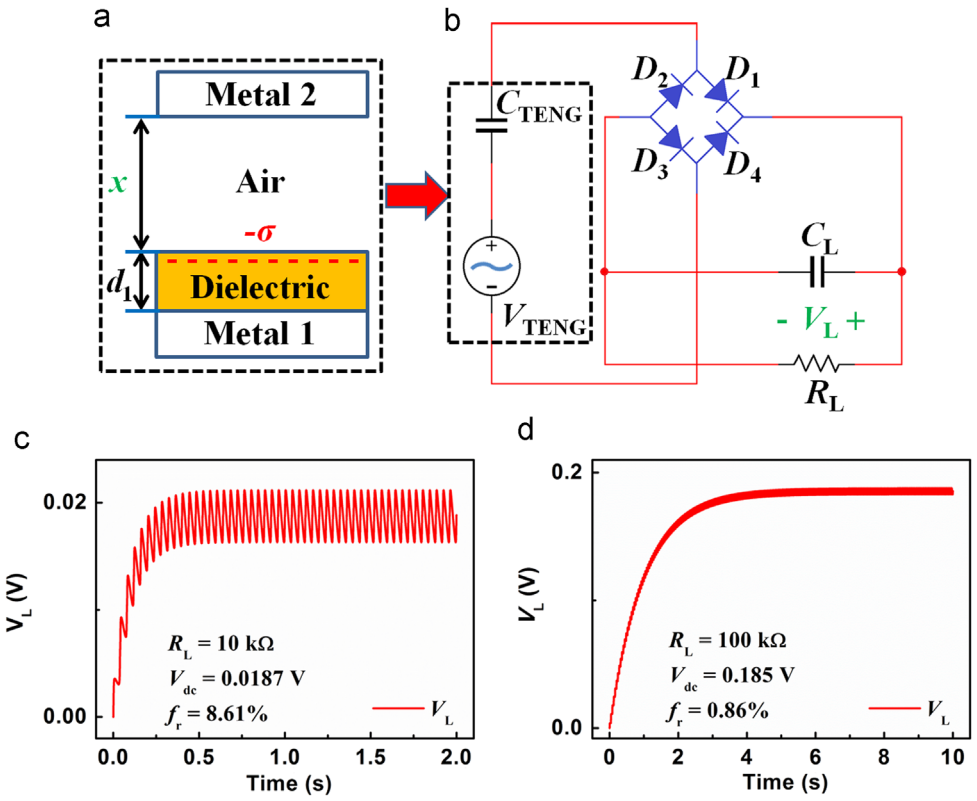

Figure 3 Output performance of the TENG system with power management circuits. (a) Structure of the TENG utilized in this calculation. (b) Equivalent circuits of the whole TENG system. (c) Real-time output voltage curve under C_L=10 μF and R_L=10 kΩ conditions. (d) Real-time output voltage curve under C_L=10 μF and R_L=100 kΩ conditions.

the limitation of the maximum voltage that the TENG can provide, V_{DC} gets to its saturation value when R_L is large enough. V_{DC} has a small dependence on C_L when R_L is very small. When R_L increases a little bit (larger than 10 kΩ in this case), v_{ripple} becomes negligible comparing to V_{DC}. At the same time, V_{DC} becomes independent of C_L. This is because all of the capacitance shows infinite impedance at DC condition and the total impedance of the parallel between R_L and C_L is always R_L. Since V_{DC} only depends on R_L and has almost no dependence on C_L, the average power is also only dependent on R_L, as shown in Figure 4b. Same as the case in the simple resistive load, there also exists an optimum R_L at which the largest average DC power is reached, which is because of the impedance match between the load and the TENG. As C_L has almost no impact on V_{DC}, both the average power curve and the optimum R_L are also independent of C_L. However, different from V_{DC} and the average power, f_r depends on both R_L and C_L, and decreases when either R_L or C_L increases. This phenomenon results from the increase of the decay time constant of such load circuit, which equals to the product of R_L and C_L. Therefore, it seems that larger C_L is good for the whole performance of the circuit because it has no influence on V_{DC} but can largely reduce f_r. However, larger C_L will increase the length of the transition state and make it more difficult to reach the steady state, when the whole circuits begin to function. As shown in Figure 4d, for the same R_L, it takes less than 5 s to reach steady state when C_L is only 10 μF while it takes about 50 s to reach steady state when C_L is 100 μF. This is because larger capacitance will require larger amount of charges to reach the same final voltage.

From the discussion above, we can obtain the following strategy for the design of the power management system. First, simulate the whole system with a relative large C_L and different R_L to obtain the optimum resistance. Second, setting R_L at the optimum resistance, simulate the whole system with different C_L and calculate the f_r-C_L curve. Third, from the requirement of real application on f_r and the calculated f_r-C_L curve, choose a minimum C_L that meets the requirement for f_r. Finally, from the optimum resistance and the load resistance for the real application, design a DC-DC convertor to realize load adaption. From the above procedures, a power management system for TENG can be easily designed.

Conclusion

In summary, the first equivalent circuit model was proposed and the first integrated simulator for triboelectric nanogenerator systems is built from this equivalent circuit model and validated through comparison with the analytical results. Utilizing this simulator, we analyzed the performance of a whole system containing TENG and power management circuits. The DC voltage output is only affected by the load resistor and is almost independent of the filter capacitor. Increasing the load resistor can help increase the DC voltage output but there exists an optimum

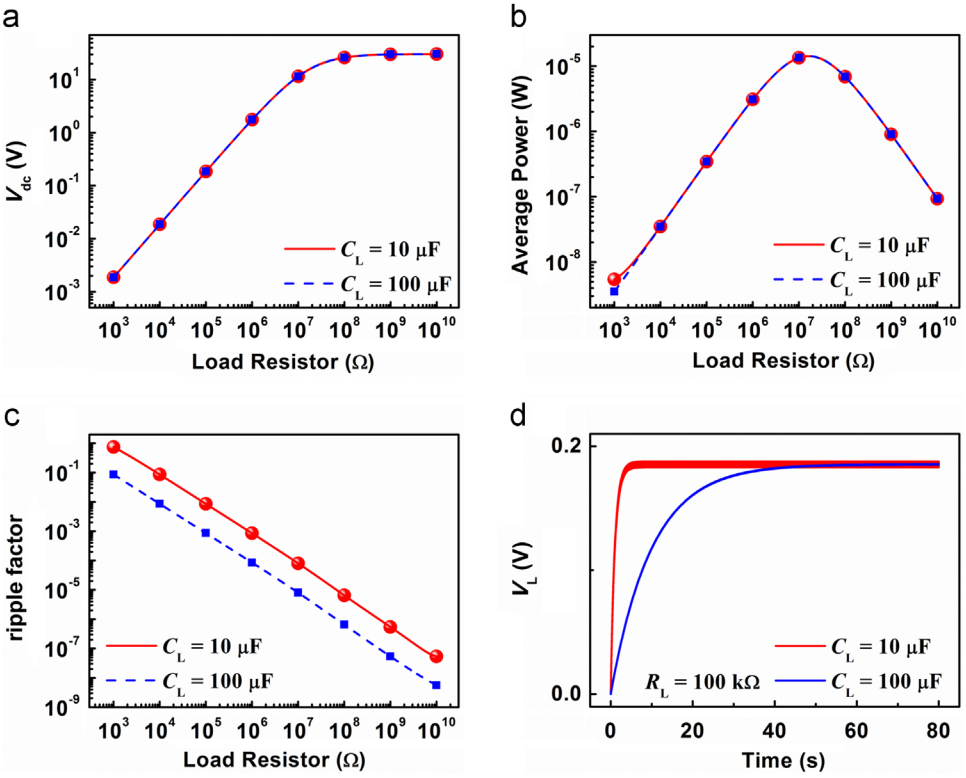

Figure 4 Optimization of the performance of the integrated TENG system. (a) DC voltage under different load resistances and filter capacitances. (b) Average output power under different load resistances and filter capacitances. (c) Ripple factor under different load resistances and filter capacitances. (d) Real-time output voltage curve under 100 kΩ load resistance and different filter capacitances.

load resistance at which the energy delivered gets its maximum. The ripple factor of the output is determined by the product of the load resistance and the filter capacitance. Increasing either of them can reduce the ripple factor, but large capacitor will lead to a longer transition state. Based on the above conclusion, we provide the design flow for such power management system. This new simulation method is a standard tool and method of TENG simulation, which can be applied to any TENG systems. It will greatly facilitate the future design and optimization of TENGs. In addition, the discussion of the power management circuit can serve as a guide in next-step experiments for real applications.

Acknowledgment

This research was supported by U.S. Department of Energy, Office of Basic Energy Sciences under Award DEFG02-07ER4 6394, MANA, the World Premier International Research Center Initiative (WPI Initiative), MEXT, Japan.

Appendix A. Supporting information

Supplementary data associated with this article can be found in the online version at http://dx.doi.org/10.1016/j.nanoen.2014.05.018.

References

[1] Y. Suzuki, IEEJ Trans. Electr. Electron. 6 (2011) 101–111.
[2] C.R. Saha, T. O'Donnell, N. Wang, R. McCloskey, Sens. Actuators A 147 (2008) 248–253.
[3] A. Lal, R. Duggirala, H. Li, IEEE Pervas. Comput. 4 (2005) 53–61.
[4] S.P. Beeby, R.N. Torah, M.J. Tudor, P. Glynne-Jones, T. O'Donnell, C.R. Saha, S. Roy, J. Micromech. Microeng. 17 (2007) 1257–1265.
[5] J.D. Chen, D. Chen, T. Yuan, X. Chen, Appl. Phys. Lett. 100 (2012) 213509.
[6] R.G. Horn, D.T. Smith, A. Grabbe, Nature 366 (1993) 442–443.
[7] H.T. Baytekin, A.Z. Patashinski, M. Branicki, B. Baytekin, S. Soh, B.A. Grzybowski, Science 333 (2011) 308–312.
[8] L.S. McCarty, G.M. Whitesides, Angew. Chem. Int. Ed. 47 (2008) 2188–2207.
[9] F.R. Fan, Z.Q. Tian, Z.L. Wang, Nano Energy 1 (2012) 328–334.
[10] X.S. Zhang, M.D. Han, R.X. Wang, F.Y. Zhu, Z.H. Li, W. Wang, H.X. Zhang, Nano Lett. 13 (2013) 1168–1172.
[11] S.H. Wang, L. Lin, Y.N. Xie, Q.S. Jing, S.M. Niu, Z.L. Wang, Nano Lett. 13 (2013) 2226–2233.
[12] L. Lin, S.H. Wang, Y.N. Xie, Q.S. Jing, S.M. Niu, Y.F. Hu, Z.L. Wang, Nano Lett. 13 (2013) 2916–2923.
[13] S.H. Wang, Z.H. Lin, S.M. Niu, L. Lin, Y.N. Xie, K.C. Pradel, Z.L. Wang, Acs Nano 7 (2013) 11263–11271.
[14] S. Kim, M.K. Gupta, K.Y. Lee, A. Sohn, T.Y. Kim, K.S. Shin, D. Kim, S.K. Kim, K.H. Lee, H.J. Shin, D.W. Kim, S.W. Kim, Adv. Mater. 26 (2014) 3918–3925.
[15] Y.S. Zhou, G. Zhu, S.M. Niu, Y. Liu, P. Bai, Q.S. Jing, Z.L. Wang, Adv. Mater. 26 (2014) 1719–1724.
[16] S.M. Niu, S.H. Wang, L. Lin, Y. Liu, Y.S. Zhou, Y.F. Hu, Z.L. Wang, Energy Environ. Sci. 6 (2013) 3576–3583.

[17] S.M. Niu, Y. Liu, S.H. Wang, L. Lin, Y.S. Zhou, Y.F. Hu, Z.L. Wang, Adv. Mater. 25 (2013) 6184–6193.
[18] S.M. Niu, Y. Liu, S.H. Wang, L. Lin, Y.S. Zhou, Y.F. Hu, Z. L. Wang, Adv. Funct. Mater. 24 (2014) 3332–3340.
[19] S.M. Niu, S.H. Wang, Y. Liu, Y.S. Zhou, L. Lin, Y.F. Hu, K.C. Pradel, Z.L. Wang, Energy Environ. Sci. 7 (2014) 2339–2349.
[20] J.J. Ebers, J.L. Moll, Proc. I.R.E. 42 (1954) 1761–1772.
[21] E. Lefeuvre, A. Badel, C. Richard, D. Guyomar, J. Intell. Mater. Syst. Struct. 16 (2005) 865–876.

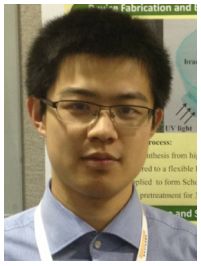

Simiao Niu is a Ph.D. candidate working as a graduate research assistant in School of Materials Science and Engineering at the Georgia Institute of Technology, under the supervision of Prof. Zhong Lin Wang. He earned his B.E. degree in the Institute of Microelectronics at Tsinghua University in 2011 with the highest honors and outstanding undergraduate thesis award. His doctoral research interests include theoretical and experimental studies on: mechanical energy harvesting by triboelectric nanogenerators and high-performance piezotronic and piezo-phototronic sensors based on piezoelectric nanowires.

Yu Sheng (Alvin) Zhou is a Ph.D. candidate supervised by Prof. Zhong Lin (Z.L.) Wang in School of Materials Science and Engineering at the Georgia Institute of Technology. He received his B.S. in Applied Physics and M.S. in Applied Optics from Beihang University (BUAA). His doctoral research focuses on mechanical energy harvesting and self-powered sensors, scanning probe microscopic study on electro-mechanical coupling (eg. piezotronics) in nano-structured semiconductor materials as well as triboelectrification between metal and dielectric materials.

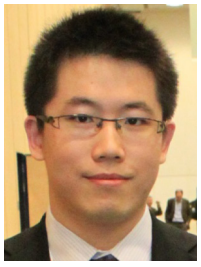

Dr. Sihong Wang is a postdoctoral fellow in Prof. Zhong Lin (Z.L.) Wang's group at the Georgia Institute of Technology. He obtained his Ph.D. degree in Materials Science and Engineering from the Georgia Institute of Technology in 2014 under the supervision of Prof. Zhong Lin (Z.L.) Wang, and his B.S. in Materials Science and Engineering from Tsinghua University, China in 2009. His research mainly focuses on nanomaterial-based mechanical energy harvesting and energy storage, self-powered systems, nanogenerator-based sensors and piezotronics.

Ying Liu received her B.S. in physics from the Yuanpei program at Peking University in 2009 and is a Ph.D. candidate with Prof. Zhong Lin Wang in School of Materials Science and Engineering at the Georgia institute of Technology. Her main research interest is the coupling of mechanics, electronics, and photonics in the same material, which includes piezo-phototronics and triboelectrics.

Long Lin received his B.S. in Materials Science and Engineering from Tsinghua University, China in 2010. He is currently a Ph. D. candidate in School of Materials Science and Engineering at the Georgia Institute of Technology. He is working as a graduate research assistant at Prof. Zhong Lin Wang's group. His research mainly focuses on nanomaterial synthesis and characterization, fabrication of high-output nanogenerators, self-powered nanosystems, piezo-tronic and piezo-phototronic effect of semiconductor nanostructures and various applications.

Dr. Yoshio Bando is an adjunct professor at University of Tokyo in Japan. He has been working on synthesizing new one-dimensional inorganic nanomaterials, and clarifying their structures and properties. By utilizing sophisticated TEM, he has discovered many new nanotubes and nanowires such as BN, MgO, and AlN. He has received many outstanding awards such as the Tsukuba Prize in 2005, Academician, World Academy of Ceramics in 2004, Commendation Award by the Minister of State for Science and Technology in 1998, Academic Award of the Ceramic Society of Japan in 1997, Seto Award of Electron Microscopy Society of Japan in 1994, Science and Technology Accomplishment Award by the Minister of State for Science and Technology in 1994. In 2002, he was chosen as one of the "Top Thirty Key Persons in Nanotechnology" in Japan by the scientific journal, "Nikkei Science". He is appointed as adjunct member of the Science Council of Japan (2006). He is now a Fellow of American Ceramic Society and an Editor-in-Chief of Journal of Electron Microscopy.

Dr. Zhong Lin Wang is a Hightower Chair and Regents's Professor at the Georgia Institute of Technology. He is also the Chief scientist and Director for the Beijing Institute of Nanoenergy and Nanosystems, Chinese Academy of Sciences. His discovery and breakthroughs in developing nanogenerators establish the principle and technological road map for harvesting mechanical energy from environment and biological systems for powering personal electronics. He coined and pioneered the field of piezotronics and piezo-phototronics by introducing piezoelectric potential gated charge transport process in fabricating new electronic and optoelectronic devices. This historical breakthrough by redesign CMOS transistor has important applications in smart MEMS/NEMS, nanorobotics, human-electronics interface and sensors. Dr. Wang's entire publications have been cited for over 60,000 times. The H-index of his publications is 129.